Data-driven generator of stochastic dynamic loading due to people bouncing

Vitomir Racic [a,b,*], Jun Chen [c,1]

[a] Department of Civil and Structural Engineering, University of Sheffield, Sir Frederick Mappin Building, Sheffield S1 3JD, United Kingdom
[b] Department of Civil and Environmental Engineering, Politecnico di Milano, Piazza Leonardo da Vinci 32, 20133 Milan, Italy
[c] Department of Building Engineering, Tongji University, 20092 Shanghai, China

Received 23 September 2014
Accepted 12 April 2015
Available online 30 June 2015

1. Introduction

In civil engineering dynamics there has been a growing number of reported problems related to excessive vibrations of floors, staircases and assembly structures (grandstands, spectator galleries, etc.) in entertaining venues induced by active people. Significant structural motion felt in 1996 on the Manchester United's Old Trafford Stadium and their London rival Arsenal during pop concerts are the first notable problems in the UK [1]. Five years later the Cardiff showpiece Millennium Stadium needed to be stiffened to satisfy safety regulations for concert events [2], while in 2003 Leeds Town Hall had to be evacuated after only 30 min of a rock concert as a 1000-strong crowd of fans induced vibrations so large that the floor occupied visibly cracked [3]. In continental Europe alarming levels of vibrations estimated above 50%g were observed on Nürnberg football stadium in Germany [4], while on the other side of the Atlantic a similar account was given of the Maracanã stadium in Rio de Janeiro Brazil [5]. More recently, during an aerobic exercise session a group of seventeen people caused the 39-story residential–commercial building in Seoul to shake for ten minutes, prompting hundreds to flee in panic [6]. All these represent a sample of the many cases that indicate the level of uncertainty with which civil structural engineers are faced nowadays when designing entertaining venues, which naturally require vibration performance assessment under human-induced excitation.

The main cause of this unsatisfactory situation is that structures are becoming more flexible. Substantial developments in work-manship and structural materials have enabled daring architects and structural engineers to promote more slender designs than previously. These reduce the mass and stiffness of a structure, hence it is more likely to have a natural frequency within the typ-ical range of rates of repetitive body motion of active occupants (i.e. up to 5 Hz) yielding a large (and often resonant) dynamic response. Moreover, there is a lack of adequate design guidance relevant to crowd rhythmic excitation. BS 6399-1:1996 [7], BRE Digest 426 [8], the User's Guide to the National Building Codes of Canada [9] Commentary D (Part 4 of Division B) and ISO 10137:2007 [10] were shown to be over-conservative based upon observations of real structures [11]. The Institution of Structural Engineers (IStructE), Department for Communities and Local Government (DCLG), Department for Transport, Local Government and the Regions (DTLGR) and Department for Culture, Media and Sport (DCMS) have been closely involved with a number of UK research projects designed to address the problem [12–18] and the results have been fed into two world leading design recommendations [19,20]. Their latest design guidance on crowd dynamic loading of grandstands [20] is a step in the right direction but still not perceived as the final version. The vital

* Corresponding author at: Department of Civil and Structural Engineering, University of Sheffield, Sir Frederick Mappin Building, Sheffield S1 3JD, United Kingdom. Tel.: +44 (0) 114 222 5790; fax: +44 (0) 114 222 5718.

E-mail addresses: v.racic@sheffield.ac.uk (V. Racic), cejchen@tongji.edu.cn (J. Chen).

[1] Tel.: +86 21 6598 1505; fax: +86 21 6598 6345.

Nomenclature

f_b	bouncing rate or bouncing frequency
$F(t)$	force time history
G	body weight
α_i	dynamic load factors (DLF)
φ_i	Fourier phases
f_s	sampling rate
$T_i,\ T'_k$	cycle intervals
τ_i, τ'_k	normalised cycle intervals
μ_T	mean of T_i
$S_\tau(f_m), S'_\tau(f_n), S'_\tau(f)$	ASD of τ_i and τ'_k
Δf, $\Delta f'$	spectral spacing
$A_\tau(f_m), A'_\tau(f_n)$	Fourier amplitudes of τ_i
W_j	Gaussian heights (weights)
c_j	Gaussian centres
b	Gaussian widths
$Z(t)$	template shape
E_i, E'_k	energy of weight normalised cycles
E_{tc}	energy of template cycle
ΔE_i	disturbance term
ξ_k	scaling factor
ρ_0, ρ_1	coefficients of linear regression
ρ	correlation coefficient
N	number of cycles
T	duration of force signal

refinement should address modelling the actual nature of human activities and the corresponding loads. Although there can be no absolute certainty on the way any random group of people will behave, the guidance is grounded on a conservative deterministic representation of crowd dynamic loading. More adequate models would portray it as a stochastic process suitable for probabilistic performance-based assessment of structural vibration response. This should be done in a similar fashion as modelling wind, wave or earthquake loading has been done for decades, all of them characterised by considerable uncertainty and randomness – the feature this study specifically aims to address.

While it is widely recognised that the most severe crowd-induced loading of entertaining venues comes from jumping, it is often rightly assumed that bouncing loads are more realistic for groups and crowds in the long term. Bouncing is a typical action in response to aural stimulation and has often been described as attempting to "jump" whilst the feet remain in contact with the ground [11]. People find bouncing preferable to jumping due to the lower energy consumption [12], which makes it particularly comfortable during long concert events [20]. The magnitude of the loading is smaller and more regular in comparison to high loads from jumping [21,22], but as the subject remains in contact with the structure they can comfortably achieve a greater activity rate. For instance, Yao et al. [12] reported that bouncing frequen-cies can be as high as 4.5 or even 5 Hz. For all these reasons, the focus of the present study is on bouncing loads only.

A key ingredient of a reliable load model of bouncing crowds is a reliable model of individual bouncing forces. Measured individual force time histories are characterised by immense inter-subject variability and are invariably near-periodic [23,17], indicating their narrow band nature (Fig. 1). However, to ease design process, they are commonly assumed identical, perfectly periodic and presentable via Fourier series [20]:

$$F(t) = G\sum_{i=1}^{m}\alpha_i \cos(2\pi i f_b t - \varphi_i) \qquad (1)$$

Here $F(t)$ is the force magnitude at time t, with G representing the body weight in the same unit (most frequently N). Coefficients α_i and φ_i are the dominant Fourier amplitudes and phase angles corresponding to m integer multiples of the bouncing rate f_b (Fig. 1b). Known as "dynamic load factors" (DLFs), α_i were studied on a limited sample of bouncing force records and the results were reported in the Working Group guideline [20]. However, φ_i have been ignored (i.e. $\varphi_i = 0$) and the values have never been publicised in detail. Section 3 presents results of fitting both α_i and φ_i to the lar-gest database of experimentally measured individual bouncing force signals established in Section 2. In the context of the present study, these results are used in Section 3 to describe morphology of the bouncing force signals.

It is now widely accepted that the modelling strategy based on Fourier harmonics leads to significant loss of information during the data reduction process [24–26,22,27,28]. For example, Brownjohn et al. [25] demonstrated that neglecting the energy around dominant Fourier harmonics (Fig. 1b), which is a result of uneven footfalls, yields up to 50% error in predicted vibration response. More recent study by Van Nimmen et al. [29] showed that precision of simulated resonant vibration response primarily depends on whether variability of timing between successive footfalls is taken into account. A model of variability of successive bouncing intervals is elaborated in Section 4, while variability of the corresponding force amplitudes is presented in Section 5.

The primary objective of the present study is to build a mathematical framework that can generate the correct interface forces between individuals and the occupied structure. Key modelling parameters are carefully selected to enable model calibration against force signals recorded under a wide range of conditions. Here, it is shown how the modelling parameters can be extracted from forces generated on a flat stationary surface, hence discounting the effect of human–structure dynamic interaction [11], while the test subjects were bouncing to an auditory stimulus only. However, there is convincing evidence that environment, vibration level, age, gender and fitness, as well as different combinations of auditory, visual and tactile stimuli exert a strong influence on individuals bouncing and the resulting forces [11]. These still need to be measured and incorporated into the suggested modelling framework.

2. Experimental data collection

The data collection was carried out in the Light Structures Laboratory in the University of Sheffield, UK. A test protocol, approved by the Research Ethics Committee of the University of Sheffield, required all participants should complete a Physical Activity Readiness Questionnaire and a preliminary fitness test (measuring blood pressure and resting heart rate) to check whether they were suited to the kind of physical effort required during the experiment. Measurements of the body mass, age and height were taken for test subject who passed the fitness test. Although different types of footwear affect the force records [30], all participants wore comfortable flat shoes due to health and safety reasons.

Each participant was engaged in twelve bouncing tests, thereby generated twelve force signals. During each test a participant was asked to bounce to a steady metronome beat which was randomly selected from the frequency range 1.2–4.5 Hz with the increment of 0.3 Hz. A test lasted between 25 and 45 s, being shorter for the higher frequencies so the participant would not tire much. Rests were allowed between the tests.

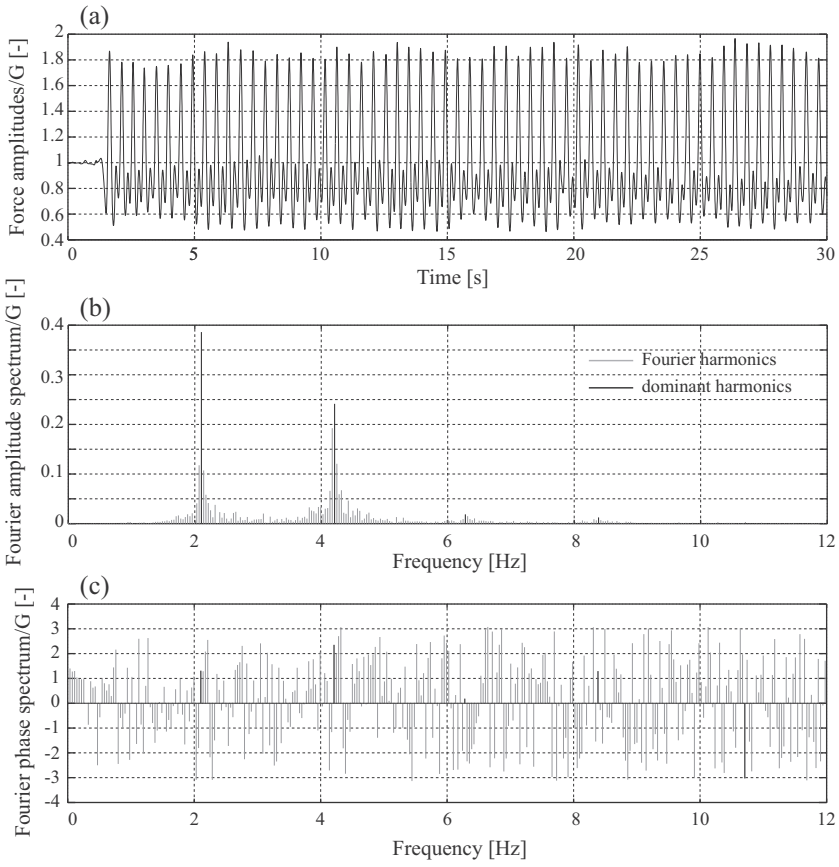

Fig. 1. Example of measured bouncing (a) force–time history and its Fourier (b) amplitude and (c) phase spectra.

The corresponding force signals were recorded by an AMTI BP-400600 force plate [31] that was rigidly fixed to the laboratory floor (Fig. 2). The signals were sampled at f_s = 200 Hz. In total, 80 volunteers (51 males and 29 females, body mass 72.7 ± 15.4 kg, height 171.2 ± 9.2 cm, age 26.4 ± 7.1 years) were drawn from students, academics and technical staff of the University of Sheffield who all together generated 960 vertical bouncing force signals of kind illustrated in Fig. 3. After a visual inspection, 60 signals recorded at high bouncing rates were cast aside. This is because some test subjects struggled to follow metronome beats at the top frequency range, occasionally stopped moving and therefore generated unrepresentative force time histories.

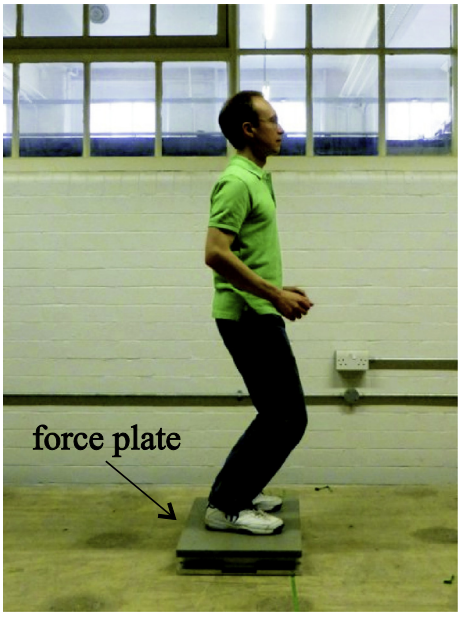

Fig. 2. Experimental setup.

In the remaining part of the paper, the so established database is used to provide a mathematical model which can reliably simulate the measurements. Sections 3–5 show how the force shape and the stochastic features of intra-subject variability of bouncing rate and force amplitudes can be extracted and modelled for a single force record. Section 6 compares simulated force signals against their measured counterpart. In Section 7 the modelling procedure presented in the previous sections is applied to all force records in the database, leading to a numerical generator of random bouncing force signals which can account for intra- and inter-subject diversity of bouncing loads.

3. Modelling shape of bouncing forces

Despite all the criticism of the Fourier approach in Section 1, Eq. (1) is not abandoned entirely in the present study. It is used to describe the "repetitive" shape of individual force signals between the successive bouncing cycles, so called "template shape". A bouncing cycle can be defined between any two nominally identical events in the force time history. Since the vertical force amplitudes oscillate around body weight of the test subject, the point where the amplitude is equal to the body weight and has a

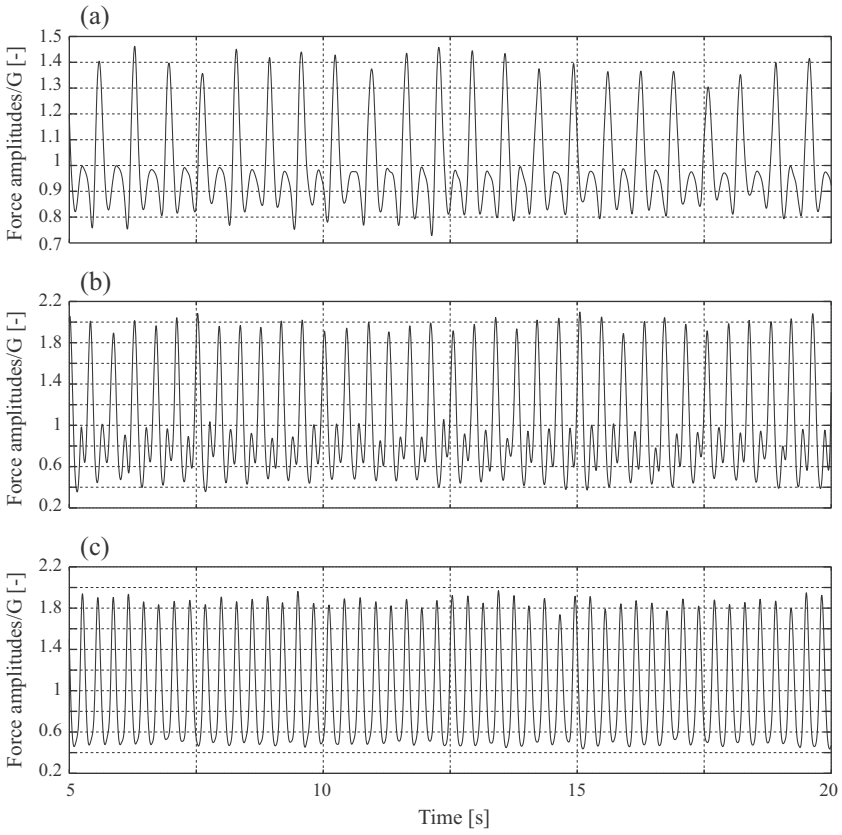

Fig. 3. Examples of bouncing force records generated at given metronome beats (a) 1.5 Hz, (b) 2.4 Hz and (c) 3.3 Hz.

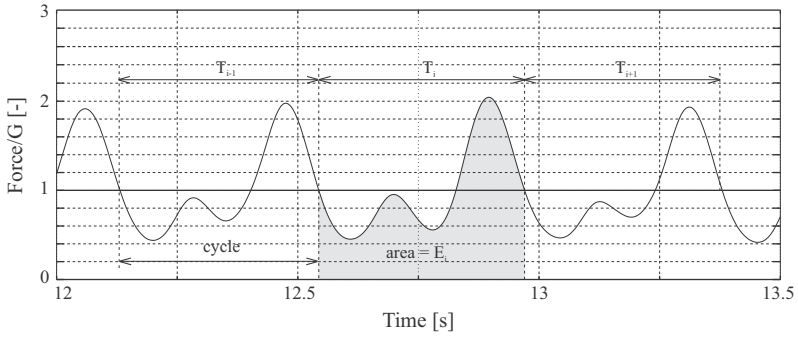

Fig. 4. A portion of the force record from Fig. 3b.

negative gradient was selected as starting (and completing) event (Fig. 4).

From the 30 s long force signal illustrated partly in Figs. 3b and 4 and yielding about 70 cycles, the central portion comprising 66 successive cycles was extracted for further analysis. Four cycles (i.e. approximately 5% of all cycles measured) at the beginning and the end of the force time history were discarded as unreliable since their natural variability might have been affected by the measuring process.

The selected 66 cycles have been normalised by the body weight G, lined up at their origins and resampled to f_s/f_b data points. Fig. 5 confirms that there is a common shape (here called "template" shape) that nonlinearly distorts along time and ampli-tude axes on the cycle-by-cycle basis. Due to misalignments of the

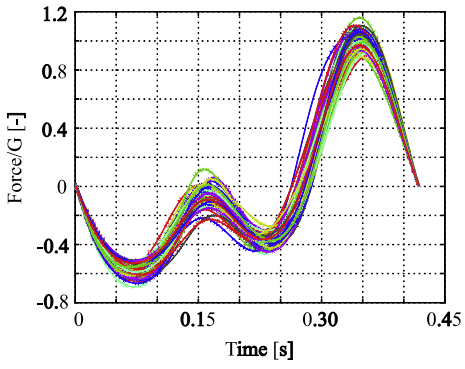

Fig. 5. Resampled G-normalised cycles for DTW.

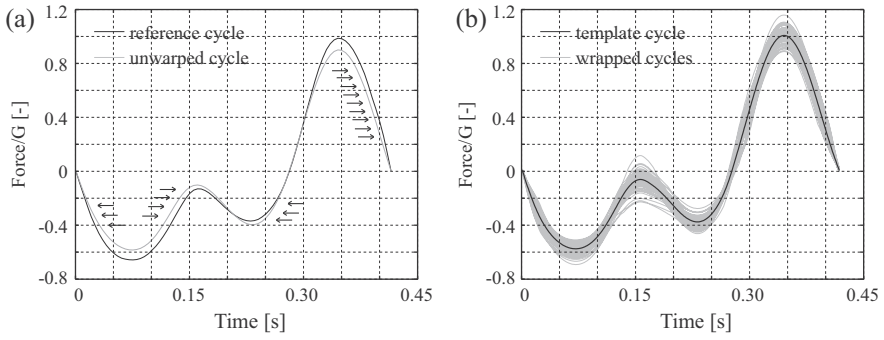

Fig. 6. (a) Illustration of DTW, and (b) template cycle.

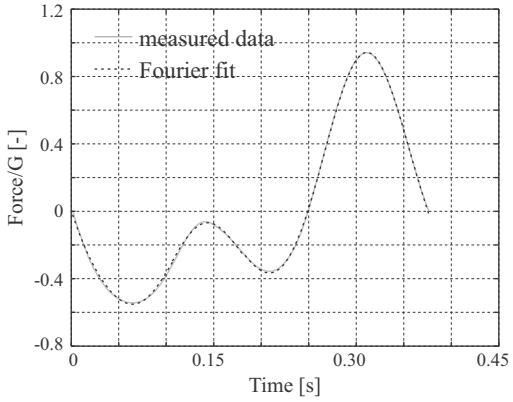

Fig. 7. Fitting the template shape.

common events along the time axis, such as positions of the local extreme values, point-by-point numerical average over the actual 66 cycles would be a poor representation of the template shape. Hence, the average was calculated after the common events had been aligned using dynamic time warping (DTW), a method commonly used in iris scans, finger print and voice recognition [32]. The DTW nonlinearly shifts common events (Fig. 6) while minimising the sum of squared differences between their amplitudes [33]. Although wavelet analysis might look as easier option, note that "mother" wavelets can be only linearly scaled [34].

Since the DTW can warp only two signals at a time, 65 of the 66 cycles were warped individually onto a "reference cycle" (Fig. 6). It is one of the actual 66 cycles that minimises the sum of point-by-point Euclidean distances to their simple numerical point-by-point average [35]. The resulting warped cycles and the template shape are shown in Fig. 6b.

The shape of the template cycle $Z(t)$ can be described as a sum of its first four Fourier harmonics (Eq. (2)). The results of the curve fitting are summarised in Fig. 7 and Table 1.

Table 1
Results of curve fitting the template shape $Z(t)$.

Parameters	f_b = 2.40 Hz			
	i = 1	i = 2	i = 3	i = 4
α_i (–)	0.55	0.42	0.07	0.02
φ_i (rad)	−1.18	−1.85	2.26	2.58

$$Z(t) = \sum_{i=1}^{4} \alpha_i \cos(2\pi i f_b t - \varphi_i) \tag{2}$$

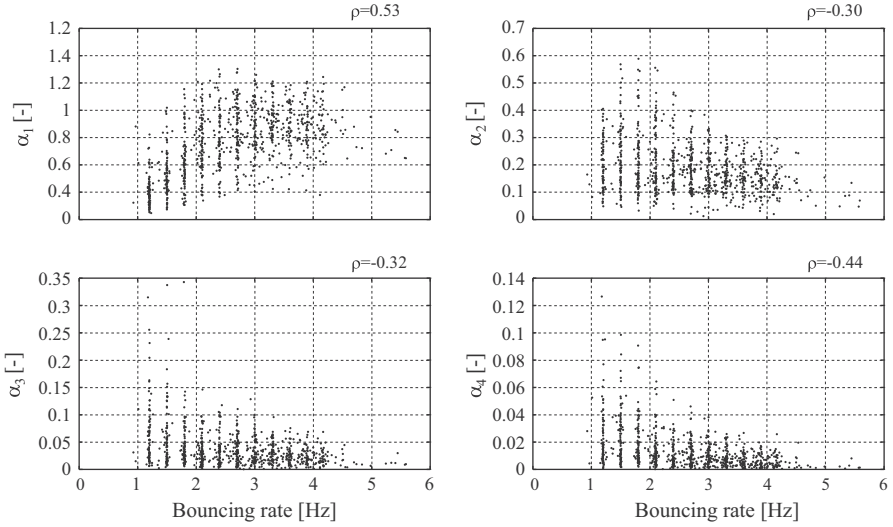

Fig. 8. DLFs vs. bouncing rate.

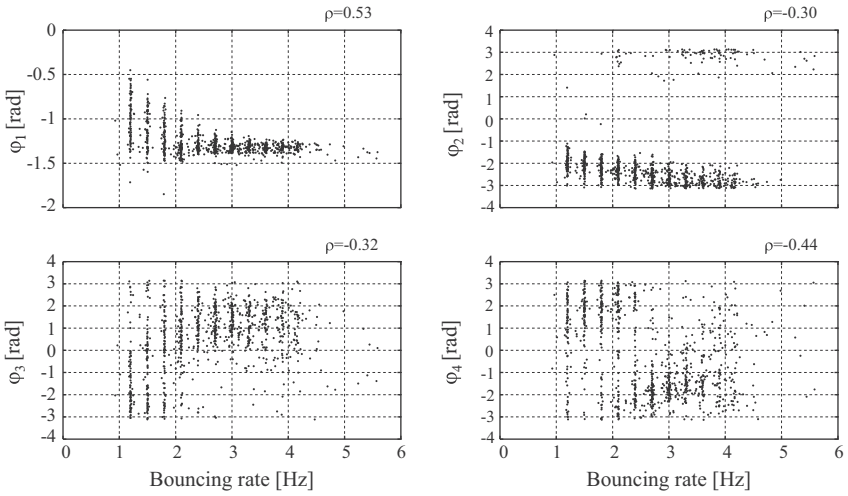

Fig. 9. Fourier phases vs. bouncing rate.

Table 2
Mean value and (standard deviation) of α_i and φ_i at different bouncing rates.

f_b (Hz)	α_1 (–)	α_2 (–)	α_3 (–)	α_4 (–)	φ_1 (rad)	φ_2 (rad)	φ_3 (rad)	φ_4 (rad)
1.2	0.23 (0.12)	0.20 (0.09)	0.06 (0.05)	0.02 (0.02)	−1.01 (0.24)	−2.0 (0.40)	−1.16 (1.65)	0.76 (1.67)
1.5	0.33 (0.17)	0.23 (0.11)	0.05 (0.05)	0.02 (0.02)	−1.15 (0.31)	−2.11 (0.44)	−0.53 (1.74)	1.39 (1.34)
1.8	0.43 (0.20)	0.23 (0.12)	0.04 (0.03)	0.02 (0.01)	−1.20 (0.18)	−2.20 (0.68)	−0.03 (1.70)	0.86 (1.87)
2.1	0.57 (0.21)	0.21 (0.11)	0.04 (0.03)	0.02 (0.01)	−1.29 (0.13)	−1.82 (1.57)	0.49 (1.38)	0.49 (2.11)
2.3	0.58 (0.23)	0.20 (0.09)	0.04 (0.03)	0.01 (0.01)	−1.29 (0.09)	−2.35 (0.70)	1.03 (1.22)	−0.61 (1.97)
2.7	0.65 (0.21)	0.19 (0.08)	0.03 (0.02)	0.01 (0.01)	−1.31 (0.07)	−2.39 (0.90)	1.09 (0.99)	−1.32 (1.45)
3.0	0.66 (0.19)	0.17 (0.08)	0.03 (0.02)	0.01 (0.01)	−1.32 (0.06)	−2.31 (1.34)	1.30 (0.77)	−1.45 (0.82)
3.3	0.68 (0.17)	0.17 (0.06)	0.03 (0.02)	0.01 (0.01)	−1.31 (0.05)	−2.01 (1.91)	1.15 (0.98)	−1.07 (1.14)
3.6	0.68 (0.17)	0.16 (0.06)	0.03 (0.02)	0.01 (0.01)	−1.32 (0.05)	−1.64 (2.27)	1.08 (0.93)	−1.09 (1.12)
3.9	0.67 (0.17)	0.15 (0.06)	0.03 (0.02)	0.01 (∼0)	−1.33 (0.05)	−1.68 (2.25)	1.06 (1.22)	−0.61 (1.51)
4.2	0.68 (0.18)	0.15 (0.06)	0.02 (0.02)	0.01 (0.01)	−1.32 (0.04)	−1.25 (2.58)	0.95 (1.10)	−0.58 (1.66)
4.5	0.74 (0.17)	0.16 (0.06)	0.02 (0.01)	0.01 (0.01)	−1.32 (0.03)	−1.42 (2.75)	0.19 (1.66)	−1.11 (1.80)

All attempts to develop a general model of the template shape for all individuals and across all measured bouncing rates had gone awry. The results of fitting Eq. (2) to the database established in Section 2 indicate the sheer randomness of bouncing force records and a lack of strong correlation between the bouncing rates and Fourier amplitudes α_i (Fig. 8) and phases φ_i (Fig. 9). Mean values and standard deviations reported in Table 2 are derived using α_i and φ_i coefficients that correspond to 0.3 Hz wide frequency clusters which centres match the 12 bouncing rates given to the test subjects during the data collection (Section 2). For example, the cluster which centre is at 2.1 Hz contains α_i and φ_i of all force records which fundamental frequency is within the range 1.95–2.25 Hz. Figs. 8 and 9 and Table 2 clearly demonstrate inadequacy of the deterministic model adopted in the Working Group design guideline. However, in the context of the present study the results helped justify the choice of the random force model elaborated in Section 7.

Section 6 shows how the template shape can be scaled while creating successive cycles of a synthetic force–time history to reflect the variability of timing and amplitudes present in the actual force record. Modelling the variations between the succes-sive cycle intervals and their amplitudes precedes in the next two sections.

4. Variability of bouncing intervals

Variability of the consecutive cycle intervals T_i ($i = 1, \ldots, 66$) can be represented by a dimensionless series τ_i:

$$\tau_i = \frac{T_i - \mu_T}{\mu_T} \qquad \mu_T = mean(T_i) \tag{3}$$

Mean of τ_i is zero and its auto spectral density (ASD) can be cal-culated as [34]:

$$S_\tau(f_m) = \frac{A_\tau^2(f_m)}{2\Delta f}, \quad f_m = \frac{m}{66}, \quad m = 0, \ldots, 32 \tag{4}$$

where $A_\tau(f_m)$ is a single-sided discrete Fourier amplitude spectra and $\Delta f = 1/66$ is the spectral line spacing (Fig. 10). Although the

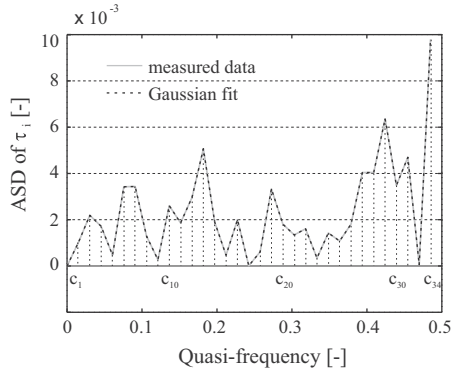

Fig. 10. ASD of τ_i series and its curve fit.

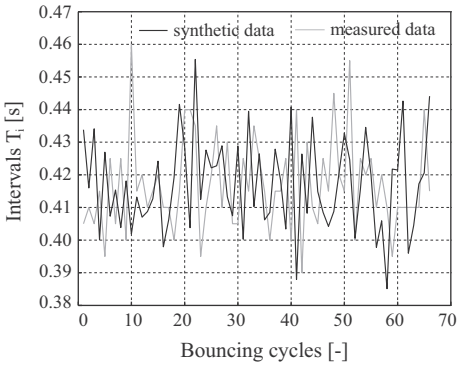

Fig. 11. Measured and an example of synthetic cycle intervals.

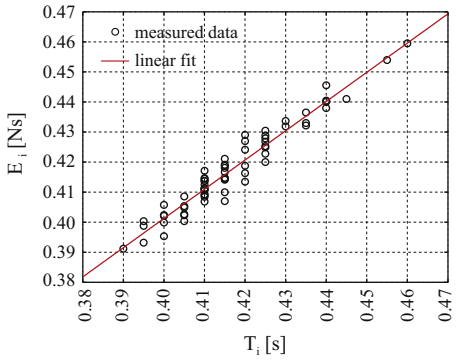

Fig. 12. Cycle energy E_i vs. cycle intervals T_i.

ASD does not depend on the length of τ_i series, more data points might reveal a smoother and very likely a richer ASD structure. However, the Research Ethics Committees in the University of Sheffield limited length of the force records due to ethical reasons.

The variance of τ_i is the integral of the ASDs [34]. Unlike random number generators, such as probability density functions, the ASD contains information of the frequency content of τ_i series, i.e. the "pattern" of variation between the consecutive τ_i values. Therefore, assuming that for a given bouncing rate a test subject maintains the same bouncing style for any period of bouncing, a model of the ASD can be used to synthesise artificial $\tau'_k (k = 1, \ldots, N)$ series of arbitrary length (e.g. $N \gg 66$) with the statistical properties of the actual τ_i series. Empirical evidence is provided in Section 6.

The ASD $S_\tau(f_m)$ can be analytically described by a sum of 33 equidistant Gaussians (Fig. 10):

$$S'_\tau(f) = \sum_{j=1}^{33} W_j e^{-\frac{(f-c_j)^2}{2b^2}} \tag{5}$$

If the Gaussian centres c_j are placed in each data point on the quasi-frequency axis and all Gaussian bells have the same predefined widths $b = \Delta f$, their heights W_j can be optimised using the non-linear least-square method [36] to fit exactly the actual ASD (Fig. 10).

To create a series of synthetic cycle intervals $T'_k (k = 1, \ldots, N)$, Eq. (5) first calculates $S'_\tau(f_n)$ values at equidistant data points $f_n = n\Delta f'$, where $n = 0, \ldots, N/2 - 1$ and $\Delta f' = 1/N$. These are then used in Eq. (4) to compute the corresponding Fourier amplitudes $A'_\tau(f_n) = \sqrt{2\Delta f' S'_\tau(f_n)}$. Assuming the uniform distribution of the phase angles in the range $[-\pi, \pi]$, $A'_\tau(f_n)$ are then fed into the inverse FFT algorithm to generate τ'_k series. Different τ'_k series with the same variance and the frequency content can be created by varying the sets of random phase angles. Finally, multiplying τ'_k by μ_T and adding the offset μ_T, yields a synthetic T'_k series (Fig. 11). Working under assumption that a test subject keeps the same bouncing style in a narrow range of bouncing rates, μ_T can take a slightly different value μ'_T to generate cycle intervals corresponding to rate $1/\mu'_T$. This is an important aspect of modelling strategy described in Section 7.

5. Variability of force amplitudes

Energy of bouncing cycles E_i can be defined as the integral of the weight-normalised force amplitudes over the corresponding cycle intervals T_i (Fig. 4).

The relationship between the two parameters (Fig. 12) can be described by the following linear regression model:

$$E_i = \rho_1 T_i + \rho_0 + \Delta E_i \tag{6}$$

Parameters $\rho_1 = 0.972$ and $\rho_0 = 0.012$ are regression coefficients and ΔE_i is a disturbance term, typically modelled as a random Gaussian noise [37].

Hence, having generated synthetic cycle intervals T'_k ($k = 1, \ldots, N$) as explained in Section 4, the corresponding energies E'_k can be calculated using Eq. (6). The energies are then assigned to a sequence of N bouncing cycles by scaling the amplitudes of the template shape with factors ξ_k:

$$\xi_k = \frac{E'_k}{E_{tc}} \tag{7}$$

where E_{tc} is the energy of the template shape. The empirical evidence is provided in the next section.

6. Synthetic force signals

This section integrates the models of template shape (Section 3), variability of the cycle intervals (Section 4) and variability of force amplitudes (Section 5) to generate an example of synthetic individual force signal. Comparison of Figs. 13a–b and 14a–b highlights the close match with the actual force record in both time and frequency domains.

The likelihood of creating two identical synthetic forces is minimal since T'_k and E'_k are random variables. However, artificial signals generated using the modelling parameters extracted from the same force measurement are statistically equivalent. This is because the morphology of bouncing cycles is controlled by the common template shape $Z(t)$, cycle intervals T'_k are created from the same ASD, which further implies the statistical equivalence of energies E'_k and force amplitudes due to the linear regression given by Eq. (6).

The next section shifts the focus of the study from a single individual to a wide human population, where individuals are considered as unique entities and their bouncing loads described as a random narrow band process.

7. Generator of random force signals

Parameters of the template shape $Z(t)$, the ASD $S'_\tau(f)$, disturbance term $\Delta E_i(t)$ and the regression coefficients ρ_1 and ρ_0, were extracted from each of the 900 force signals recorded in Section 2 and stored in 900 MATLAB structure files [38], here called "mat files". As in Section 3, the mat files were classified into the 0.3 Hz wide clusters which centres correspond to the 12 bouncing rates in the range 1.2–4.5 Hz (Table 2). Assumption that a person would generate very similar force signals when bouncing at rates that are within a cluster's narrow frequency range was already

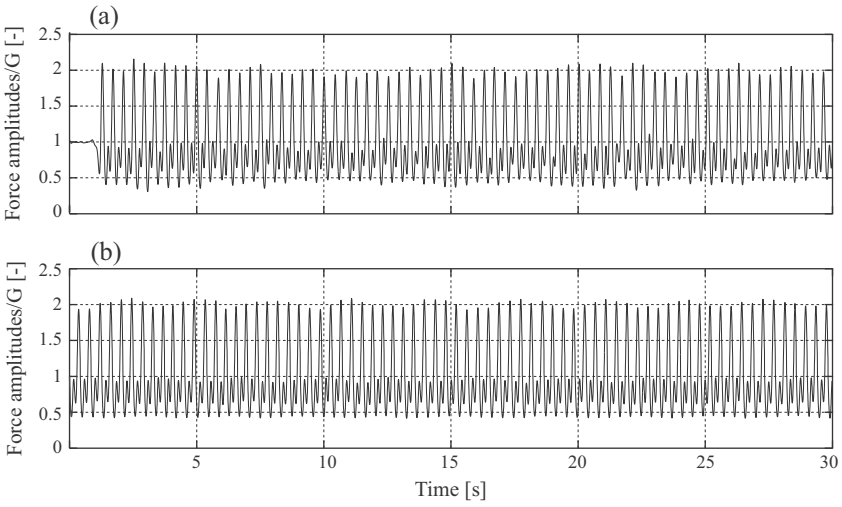

Fig. 13. (a) Measured and (b) an example of synthetic force–time series.

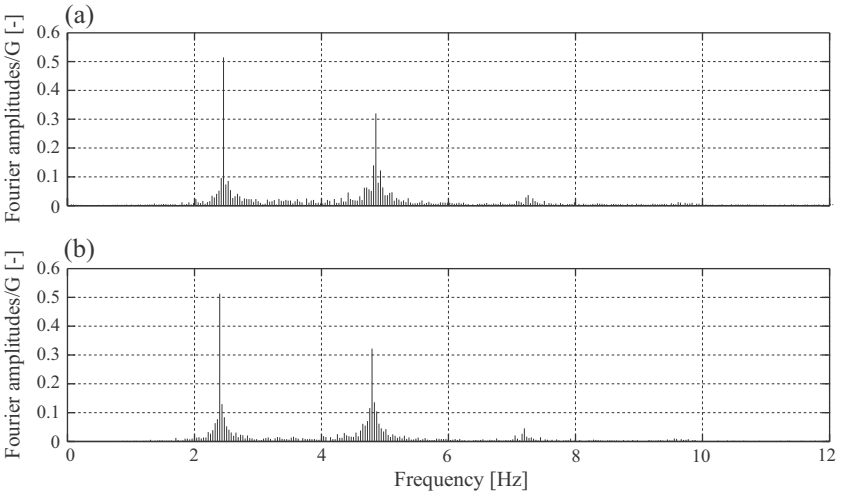

Fig. 14. Discrete Fourier amplitude spectra of the time series shown in Fig. 13.

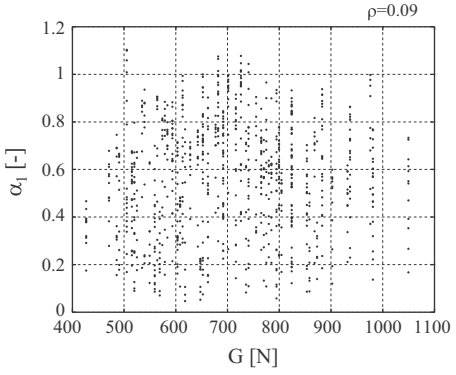

Fig. 15. Poor correlation between body weight G and the fundamental DLF α_1.

introduced in Section 4. Hence, it can be further assumed that the modelling parameters stored in any mat file within a cluster can be used to generate synthetic force signals at any bouncing rate within the cluster's frequency range. This is the key aspect of the random modelling approach adopted in this section.

The lack of correlation ($\rho = -0.09$) between the body weight G and the fundamental dynamic loading factor α_1 in Fig. 15 suggests that the body weight does not affect the force amplitudes. Hence, G values can be generated independently and randomly using probability density functions, such as reported by Hermanussen et al. [39] and Ogden et al. [40], and used to scale synthetic G-normalised force signals of a kind shown in Fig. 13b.

The flow chart in Fig. 16 presents the algorithm to generate an artificial force signal. For the preselected values of bouncing frequency f_b and duration of bouncing T, the algorithm first estimates the number of bouncing cycles $N = T * f_b$ in the signal, then rounds it up to the next integer. In the following step it selects randomly and equally likely a mat file from the frequency cluster corre-sponding to f_b. Using the modelling parameters stored in the selected file, it generates synthetic cycle intervals T_k^*, $k = 1, \ldots, N$,

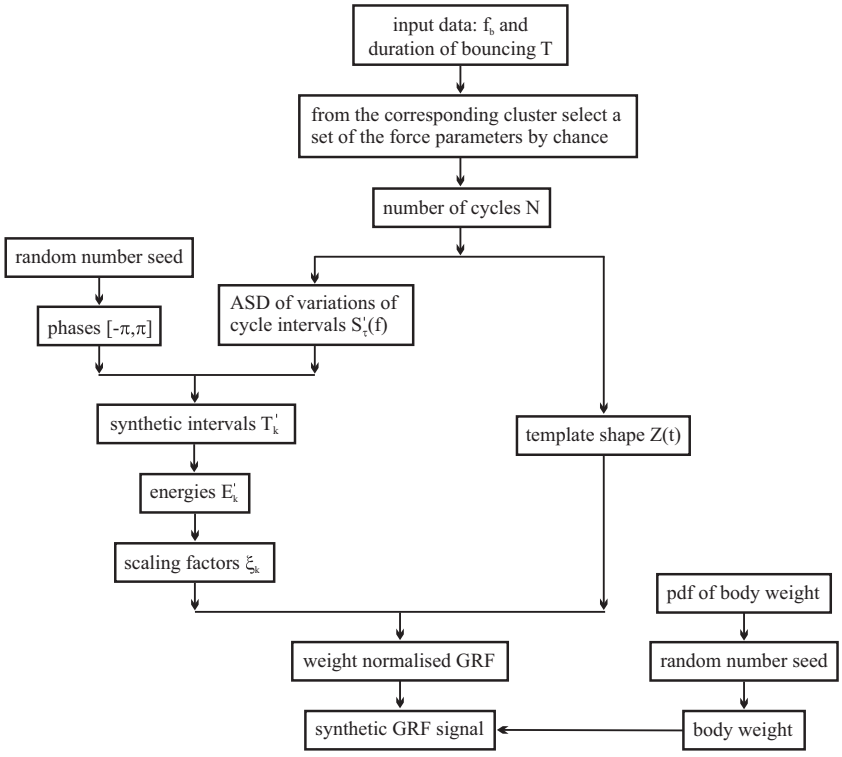

Fig. 16. Algorithm to generate a synthetic force signal.

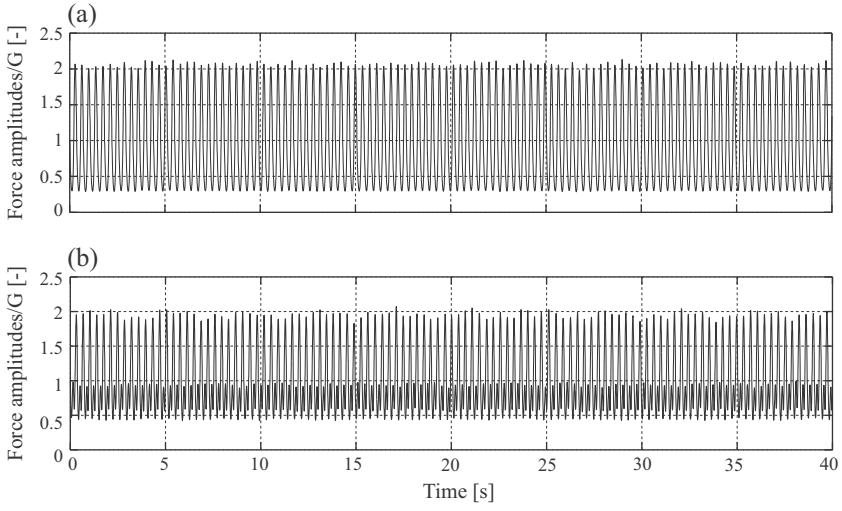

Fig. 17. Examples of artificial force signals generated for the same set of input parameters f_b = 2.7 Hz and T = 40 s.

then calculates the corresponding energies of bouncing cycles E'_k and scaling factors ξ_k. Next, the template shape $Z(t)$ is assigned to each T'_k, scaled by ξ_k and the individual cycles are aligned along the time axis. In the last step, the resulting signal is scaled by a randomly generated body weight.

Fig. 17 shows two synthetic signals generated when the model was started twice using the same input parameters f_b = 2.7 Hz and T = 40 s. The force time histories are clearly different which proves that the model can simulate the inter-subject variability. On the other hand, ability to generate signals with different degrees of the intra-subject variability is more apparent in the frequency domain (Fig. 18). The lesser spread of energy around the dominant harmonics in Fig. 18a relative to Fig. 18b indicates more regular bouncing of the first "virtual" person.

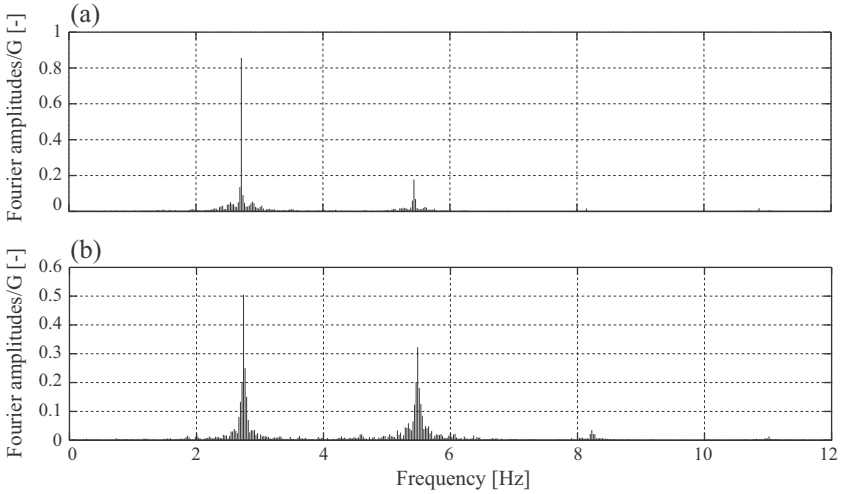

Fig. 18. Discrete Fourier amplitude spectra of the time series shown in Fig. 17.

8. Discussions and conclusions

Mainly due to the lack of fundamental data and adequate mathematical characterisation that will enable easy manual assessment of vibration response, bouncing loads are assumed in design practice as perfectly repetitive, identical for all individuals and represented by a sum of several dominant Fourier harmonics. However, increasing number of newly built structures facing vibration serviceability problems due to bouncing people clearly stressed the need of a more adequate mathematical description.

This study combines the conventional Fourier modelling approach with novel models of variability of timing and amplitudes/energy of the successive bouncing cycles, yielding a numerical generator of random near-periodic bouncing force time histories. The modelling parameters are extracted from a large database of bouncing force records, classified and stored in narrow clusters with respect to the bouncing rate. Working under assumption that forces generated at very close rates have similar shape, amplitudes and level of variability, modelling parameters within a cluster can be used to generate artificial force signals at any rate within the cluster's frequency range. The key modelling parameters are random variables, so two identical forces can be generated only by chance. This radical shift from the conservative deterministic model to a randomised and automated generator of artificial bouncing forces brings the whole field of human-induced vibrations arm to arm with dynamic analysis of structures due to other key random excitation, such as wind and earthquakes, which has been done in this way for decades. Moreover, as the model generates synthetic force signals in a fraction of a second on a standard PC configuration, it has a great potential to improve efficiency and cost-effectiveness of vibration serviceability assessment in everyday design practice.

However, there is still a room for improvement. The current version of the model runs on the parameters extracted from the force records measured on a rigid laboratory floor. Hence, it can be used to study only cases of incipient dynamic instability, i.e. when the vibration level is not too much perceptible to the occupant and therefore does not affect his/her bouncing motion. An elaborate database of bouncing force records generated by many individuals bouncing at different rates on more or less vibrating surfaces still waits to be established. Also, there are many more factors affecting human-induced loads, such as different auditory, visual and tactile stimuli, with or without the motion of the structure itself. To include them in the model, the variations in the force amplitudes, energy, timing and shape of successive bouncing cycles should be modelled as a function of dynamic response of an occupied structure, human perception to vertical vibrations and different external cues. Moreover, there is still a gap in the knowledge on the interaction between individuals in groups and crowds and its influence on the corresponding net dynamic loads on the structure. Having a dynamic model of a crowd that considers each individual as an agent bouncing and interacting with surrounding people, timing of each agent can be coupled with the proposed individual force model yielding a numerical generator of crowd bouncing loads. However, interaction between individuals within a crowd still needs to be measured and modelled.

Acknowledgements

The authors would like to acknowledge the financial support provided by the UK Engineering and Physical Sciences Research Council (EPSRC) for grants reference EP/I029567/1 (Synchronisation in dynamic loading due to multiple pedestrians and occupants of vibration-sensitive structures) and EP/K036378/1 (Advanced measurement, modelling and utilisation of bouncing and jumping loading induced by groups and crowds) as well as National Science Foundation of China (NSFC, No. 51478346). Also, the author would like to thank all test subjects for participating in the data collection.

References

[1] Rogers D. Two more 'wobbly' stands. Construction News, 17 August, 2000.
[2] Glackin M. Stadia design rethink prompted by Cardiff fiasco. Building 2000:11.
[3] Parker D. Rock fans uncover town hall floor faults. New Civil Engineer, 20 November, 2003.
[4] Kasperski M, Niemann HJ. Man-induced vibrations of a stand structure. In: Proceedings of the 2nd European conference on structural dynamics EURODYN '93, Trondheim, Norway, 21–25 June 1993.
[5] Batista RC, Magluta C. Spectator-induced vibration of Maracanã football stadium. In: Proceedings of the 2nd European conference on structural dynamics EURODYN '93, Trondheim, Norway, 21–25 June, 1993.
[6] Lee S-H, Lee K-K, Woo S-S, Cho S-H. Global vertical mode vibrations due to human group rhythmic movement in a 39 story building structure. Eng Struct 2013;57:296–305.
[7] BS 6399-1:1996. Loading for buildings. British Standard Institution, London, UK; 1996.
[8] Ellis BR, Ji T. The response of structures to dynamic crowd loads. BRE Digest 426, London, UK; 1997.
[9] Canadian Commission on Building and Fire Codes, User's Guide NBC 2005: Structural Commentaries (Part 4 of Division B). National Research Council of Canada, Institute for Research in Construction, Ottawa, Canada; 2006.
[10] International Organization for Standardization. ISO10137:2007 Bases for design of structures – serviceability of buildings and walkways against vibration, 2007.

[11] Jones CA, Reynolds P, Pavic A. Vibration serviceability of stadia structures subjected to crowd loads: a literature review. J Sound Vib 2011;330(8): 1531–66.
[12] Yao S, Wright JR, Pavic A, Reynolds P. Experimental study of human-induced dynamic forces due to bouncing on a perceptibly moving structure. Can J Civ Eng 2004;31(6):1109–18.
[13] Yao S, Wright JR, Pavic A, Reynolds P. Experimental study of human-induced dynamic forces due to jumping on a perceptibly moving structure. J Sound Vib 2006;296(1–2):150–65.
[14] Ellis BR, Littler JD. Response of cantilever grandstands to crowd loads. Part 1: serviceability evaluation. Proc ICE (Institution of Civil Engineers) Struct Build 2004;157(SB4):235–41.
[15] Duarte E, Ji T. Bouncing loads induced by an individual. In: Proceedings of the 6th European conference on structural dynamics EURODYN 2005, Paris, France, 4–7 September, 2005.
[16] Duarte E, Ji T. Action of individual bouncing on structures. J Struct Eng 2009;135(7):818–27.
[17] Parkhouse JG, Ewins DJ. Crowd-induced rhythmic loading. Struct Build 2006;159(SB5):247–59.
[18] Sim JHH, Blakeborough A, Williams M. Statistical model of crowd jumping loads. ASCE J Struct Eng 2008;134(12):1852–61.
[19] IStructE/DTLGR/DCMS Working Group. Dynamic performance requirements for permanent grandstands subject to crowd action: interim guidance on assessment and design. The Institution of Structural Engineers, London, UK; 2001.
[20] IStructE/DCLG/DCMS Working Group. Dynamic performance requirements for permanent grandstands subject to crowd action: Recommendations for management, design and assessment. The Institution of Structural Engineers, London, UK; 2008.
[21] Racic V, Pavic A. Mathematical model to generate asymmetric pulses due to human jumping. ASCE J Eng Mech 2009;135(10):1206–11.
[22] Racic V, Pavic A. Stochastic approach to modelling near-periodic jumping force signals. Mech Syst Sig Process 2010;24:3037–59.
[23] Sim JHH. Human–structure interaction in cantilever grandstands, PhD thesis. Faculty of Engineering, The University of Oxford, UK; 2006.
[24] Rainer JH, Pernica G, Allen DE. Dynamic loading and response of footbridges. Can J Civ Eng 1988;15(1):66–71.
[25] Brownjohn JMW, Pavic A, Omenzetter P. A spectral density approach for modelling continuous vertical forces on pedestrian structures due to walking. Can J Civ Eng 2004;31:65–77.
[26] Zivanovic S, Pavic A, Reynolds P. Human–structure dynamic interaction in footbridges. Bridge Eng 2005;158(BE4):165–77.
[27] Racic V, Brownjohn JMW. Mathematical modelling of random narrow band lateral excitation of footbridges due to pedestrians walking. Comput Struct 2012;90–91:116–30.
[28] Racic V, Morin JB. Data-driven modelling of dynamic excitation of bridges induced by people running. Mech Syst Sig Process 2014;43:153–70.
[29] Van Nimmen K, Lombaert G, Jonkers I, De Roeck G, Van den Broeck P. Characterisation of waking loads by 3D inertial motion tracking. J Sound Vib 2014;33(20):5212–26.
[30] Racic V, Pavic A, Brownjohn JMW. Experimental identification and analytical modelling of human walking forces: literature review. J Sound Vib 2009;326:1–49.
[31] AMTI. AMTI user manuals; 2014. <www.amti.biz>.
[32] Salvador S, Chen P. Toward accurate dynamic time warping in linear time and space. Intell Data Anal 2007;11(5):561–80.
[33] Holmes JR, Holmes W. Speech synthesis and recognition. 2nd ed. London, UK: Taylor and Francis; 2001.
[34] Newland DE. An introduction to random vibrations, spectral and wavelet analysis. 3rd ed. Harlow, UK: Pearson Education Limited; 1993.
[35] Strachan IGD. Novel probabilistic algorithms for dynamic monitoring of Electrocardiogram waveforms. In: Proceedings of the sixth international conference on condition monitoring and machinery failure prevention technologies; 2009. p. 545–55.
[36] Bates DM, Watts DG. Nonlinear regression and its applications. New York, USA: Wiley; 1998.
[37] Bishop CM. Pattern recognition and machine learning. 4th ed. New York, USA: Springer; 2006.
[38] MathWorks. Matlab user guides; 2014. <www.mathworks.com>.
[39] Hermanussen M, Danker-Hopfe H, Weber GW. Body weight and the shape of the natural distribution of weight, in very large samples of German, Austrian and Norwegian conscripts. Int J Obes 2001;25:1550–3.
[40] Ogden CL, Fryar CD, Carrol MD, Flegal KM. Mean body weight, height, and body mass index, United States 1960–2002. In: Advance data from vital and health statistics 347. Hyattsville, Maryland, USA: National Centre for Health Statistics; 2004.